MACROSCOPIC CORROSION OF STEEL THROUGH EXPERIMENTATION AND PROBABILISTIC MODELING

by

DANIEL TODD HAMPSON

(Under the Direction of Ramana M. Pidaparti)

ABSTRACT

This thesis investigates the macroscopic corrosion of steel under potentiostatic conditions using electrochemical experiments and a probabilistic modeling approach. A probabilistic cellular automata (PCA) model is developed to predict the propagation and penetration of corrosive material in the steel. The PCA model is developed in MATLAB and is corrected using experimental results from a three-electrode corrosion cell. Several steel specimens are corroded under various environmental conditions, and their mechanical strengths are evaluated. The corrected model results are evaluated using finite element analysis (FEA) and tensile testing of the experimental specimens. The trends from the FEA results correlated closely with the trends from the tensile testing, across three different specimen designs. This thesis contributes to the understanding of the corrosion behavior of steel under potentiostatic conditions and provides a tool for predicting the corrosion behavior and mechanical properties of steel under such conditions.

INDEX WORDS: probabilistic cellular automata, potentiostatic electrochemical corrosion, finite element analysis, tensile testing, macroscopic corrosion effects

MACROSCOPIC CORROSION OF STEEL THROUGH EXPERIMENTATION AND PROBABILISTIC MODELING

by

DANIEL TODD HAMPSON

B.S., The University of Georgia, 2022

A Thesis Submitted to the Graduate Faculty of The University of Georgia in Partial Fulfillment of the Requirements for the Degree

MASTER OF SCIENCE

ATHENS, GEORGIA

2023

MACROSCOPIC CORROSION OF STEEL THROUGH EXPERIMENTATION AND PROBABILISTIC MODELING

by

DANIEL TODD HAMPSON

Major Professor:	Ramana Pidaparti
Committee:	Eric Freeman
	Ramaraja Ramasamy
	Xianqiao Wang

Electronic Version Approved:

Ron Walcott
Vice Provost for Graduate Education and Dean of the Graduate School
The University of Georgia
May 2023

ACKNOWLEDGEMENTS

I would like to express my gratitude to my major professor, Dr. Pidaparti, for his invaluable guidance and advice throughout the pursuit of my master's degree. His insights and encouragement were instrumental in shaping the direction of my research and helping me overcome various challenges. I would also like to thank my peers and lab mates (Chris Altmann, Ahmet Tunc, Tyler Rush, and Will Morris) for their many contributions to the project. I would like to thank my committee members, Dr. Freeman, Dr. Ramasamy, and Dr. Wang, for their valuable feedback and support throughout the process of completing my thesis. All of these people have made contributions and insights which have greatly enhanced the quality of my work, and I am very grateful.

I am deeply indebted to my family (Dad, Mom, Nat, and Luke) for their unwavering love and support during my time at the university. Their encouragement and belief in me gave me the strength to persevere through the ups and downs of this journey. Finally, and most importantly, I would like to express my heartfelt gratitude to my wife, Maddie, for her constant love, support, and daily words of encouragement. She has been my rock, my cheerleader, and my source of inspiration throughout this journey, and I could not have done it without her.

Thank you all for your contributions and support, without which this achievement would not have been possible.

TABLE OF CONTENTS

Page

LIST OF TABLES

Page

LIST OF FIGURES

Page

CHAPTER 1

INTRODUCTION

The study of corrosion in steel is crucial in the field of materials science and engineering due to the severe impact that corrosion has on steel structures, which are essential components in various industries such as construction, transportation, and energy. According to the National Association of Corrosion Engineers (NACE), the annual cost of corrosion in the United States is estimated to be $276 billion, with the majority of these costs being attributed to the transportation, infrastructure, and energy sectors [1]. Additionally, corrosion-related failures can have serious safety implications, such as the 2007 collapse of the I-35W Mississippi River bridge in Minneapolis, which was due to corrosion-induced structural deficiencies [2].

The study of corrosion has led to the development of various techniques and methods for corrosion prevention and mitigation, including the use of coatings, inhibitors, and design modifications [3-5]. By understanding the fundamental mechanisms of corrosion and its effects on different materials, engineers and researchers can develop more effective corrosion prevention strategies and improve the reliability and safety of metal structures.

1.1 Corrosion Background and Impact on Steel Structures

Corrosion is a natural process that deteriorates the properties of materials due to their exposure to the environment. It is a pervasive issue, particularly in steel structures, where it can lead to significant economic losses, structural failure, and even human casualties. Corrosion of steel structures can occur due to various factors such as environmental conditions, mechanical stress, and

the presence of impurities [6, 7]. Corrosion not only weakens the structural integrity of steel, but it also reduces its mechanical properties, such as ductility and toughness, which may lead to catastrophic failure [8-10]. Hence, corrosion management is essential to ensure the longevity and safety of steel structures.

1.2 Motivation for the Study

Despite the importance of corrosion management, the development of effective and efficient corrosion models has remained a challenge due to the complex and stochastic nature of corrosion. Researchers have attempted to develop deterministic models to predict the rate and type of corrosion that a material may experience [11, 12]. However, this has proven difficult because there are many factors that influence corrosion, and these factors are often subject to statistical distributions [13]. For example, the environmental conditions that a material is exposed to may vary over time and space, leading to variations in the rate and type of corrosion that occurs. Similarly, the properties of the material itself, such as its microstructure, may also vary over time and space, leading to variations in its susceptibility to corrosion. Recently, probabilistic cellular automata (PCA) models have shown promise in accurately predicting the propagation of corrosion across steel surfaces [14-16]. However, further investigation is needed to optimize and validate these models for practical applications. Furthermore, these research studies focus on the nanoscopic and microscopic scales, and this study intends to focus on the macroscopic scale.

1.3 Research Objectives and Scope

The primary objective of this research is to develop a PCA model to predict the macroscopic corrosion behavior of steel under potentiostatic corrosion parameters. The focus is on optimizing and validating the PCA model using experimental data obtained from electrochemical corrosion tests and mechanical testing. The research will investigate the effect of potentiostatic corrosion

parameters such as electric potential, exposure time, and electrolyte concentration on the corrosion behavior of steel.

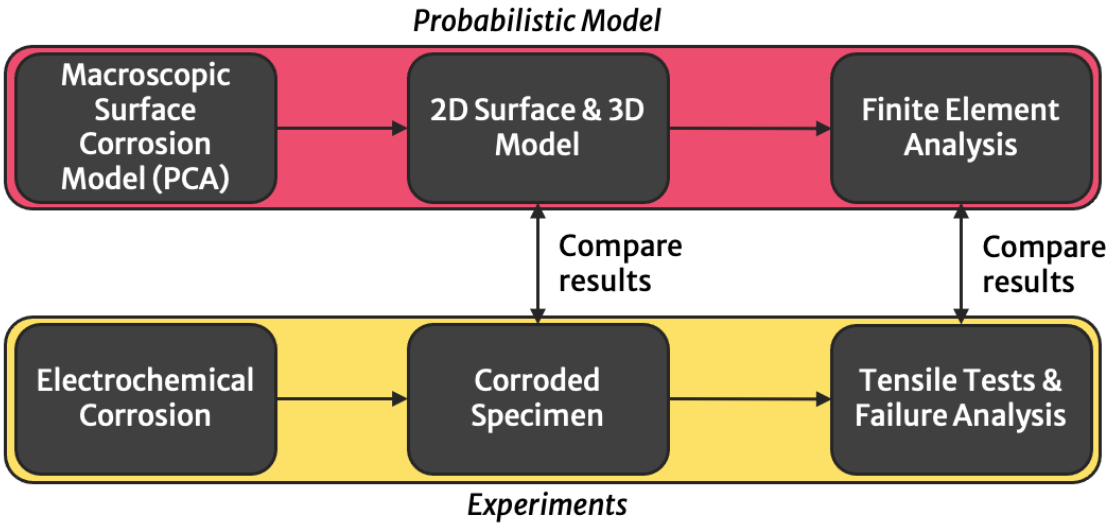

Figure 1. Scheme for corrosion modeling project.

Figure 1 depicts a flow diagram which describes the overall scheme of the project. After the PCA is developed, two comparisons will take place between the model predictions and experimental results. The first comparison will be a part of the parametric study, which is explained in-depth in §3.4. The parametric study is useful in quantifying relationships between the corrosion rate and electrochemical parameters, and these relationships are later implemented in the model. The second comparison will be a part of the mechanical evaluation of the model, which is explained in-depth in §3.5 and §3.6. The results of this comparison will evaluate whether the PCA has captured any changes in the bulk mechanical properties of the steel.

CHAPTER 2

LITERATURE REVIEW

This chapter provides an in-depth analysis of the existing research and current state-of-the-art in the field of corrosion modeling, including traditional methods such as electrochemical impedance spectroscopy and weight loss analysis, as well as emerging techniques such as the use of computational models. The chapter will also explore the various applications of cellular automata (CA) models in corrosion research, focusing specifically on probabilistic cellular automata models. This review aims to identify the research gaps and limitations of the current literature and to highlight the potential for further research in this area.

2.1 Overview of Corrosion Modeling Techniques

Over the years, researchers have developed different models to simulate corrosion processes and provide better understanding of their underlying mechanisms. The modeling techniques can be categorized into deterministic and probabilistic models. Deterministic models use mathematical equations to predict the corrosion rate based on experimental data, while probabilistic models account for the stochastic nature of corrosion phenomena.

In deterministic models, electrochemical kinetics models have been widely used to describe the corrosion process. The Tafel equation, Butler-Volmer equation, and mixed-potential theory are commonly employed in these models. For instance, Eddy et al. used the Tafel equation to model the corrosion of aluminum in an acidic medium [17], while Stipaničev et al. utilized the mixed-potential theory to investigate the corrosion behavior of carbon steel in a marine environment [18].

In probabilistic models, CA and Monte Carlo simulations are the two most commonly used methods. Stochastic CA models have been applied to model various corrosion phenomena such as pitting corrosion, stress corrosion cracking, and uniform corrosion. For example, Chen et al. used a probabilistic CA model to simulate the initiation and growth of pitting corrosion in stainless steel [19], while Caleyo et al. employed a Monte Carlo simulation to predict the corrosion initiation of carbon steel under cathodic protection [20].

Other modeling techniques include artificial neural networks (ANNs), fuzzy logic, and support vector machines (SVMs). ANNs have been used to predict the corrosion rate of metals based on various input parameters such as temperature, pH, and dissolved oxygen [21]. Fuzzy logic has been used to model the corrosion rate of ferrous pipe material in corrosive soil environments [22], while SVMs have been employed to predict the corrosion rate of steel in different seawater environments [23].

Overall, both deterministic and probabilistic models have their strengths and limitations in predicting the corrosion behavior of metallic structures. The selection of the appropriate model depends on the specific application and the available data.

2.2 Review of PCA Model Applications

Probabilistic cellular automata (PCA) is a modeling technique that has been gaining attention due to its ability to model complex and stochastic phenomena in various fields, including materials science [24-26]. PCA is a type of cellular automata that utilizes probabilities and randomness in its transition rules, allowing for the modeling of systems with inherent uncertainties and nonlinear behavior [24].

In the field of materials science, PCA has been applied to study various phenomena such as microstructure evolution, deformation behavior, and corrosion. In corrosion modeling, PCA has

been used to predict the propagation of corrosion across steel surfaces and to investigate the effect of various parameters such as pH, temperature, and inhibitor concentration on the corrosion process [15]. PCA models have also been applied in the study of other metal alloys such as aluminum, magnesium, and nickel-based alloys [14-16, 26-29].

PCA models have been used outside the field of materials science as well. For example, PCA has been utilized in ecology to model the spread of invasive species and the effect of climate change on ecosystems [30]. In computer science, PCA has been applied to modeling neural networks and simulating traffic flow [31]. Additionally, PCA has been used in economics to model financial markets and predict stock prices [32].

Overall, PCA modeling has proved to be a versatile tool with applications across various fields. The ability to model complex and stochastic phenomena with inherent uncertainties makes PCA an attractive modeling approach in materials science and beyond.

2.3 Previous Studies on PCA Modeling of Corrosion in Metal Alloys

Recently, PCA models have shown promise in accurately predicting the propagation of corrosion across metal alloy surfaces. For example, a study by Urda et al. used PCA to model the corrosion behavior of 2205 duplex stainless steel in a chloride-containing environment [27]. The results showed that the PCA model accurately predicted the development of pitting corrosion. Another study by Fatoba et al. used PCA and FEA to model the corrosion behavior of 5L X65 steel in various electrolytes [28]. The results showed that the PCA model accurately predicted the formation of corrosion products and the progression of localized corrosion.

In addition, several studies have explored the use of PCA models in combination with other techniques such as finite element analysis (FEA) and ANNs to improve the accuracy of corrosion modeling. For instance, a study by Lishchuk et al. used PCA combined with FEA to predict the

corrosion behavior of steel reinforced concrete in a chloride-containing environment [29]. The results showed that the combined model accurately predicted the corrosion depth and location. Similarly, a study by Urda et al. used PCA combined with ANNs to predict the corrosion behavior of a steel alloy in a marine environment [27]. The results showed that the combined model had a higher accuracy than the PCA model alone.

Overall, the literature suggests that PCA models have shown promise in accurately predicting the corrosion behavior of metal alloys, and the combination with other techniques can further improve their accuracy. However, more research is needed to explore the limitations and challenges of PCA modeling in different environmental and electrochemical conditions.

2.4 Review of Potentiostatic Parameters and Their Effects on Corrosion

Potentiostatic corrosion experiments allow for precise control over the electrochemical environment, making them a popular choice for studying the effects of various parameters on corrosion. Electric potential and electrolyte concentration are two critical parameters that can significantly affect the corrosion behavior of metallic materials. The literature review of the effects of these potentiostatic parameters on corrosion is essential in understanding and predicting the corrosion behavior of metallic materials in different environments.

Several studies have investigated the effect of electric potential on corrosion. It has been reported that increasing the potential difference between the metal and the electrolyte can lead to accelerated corrosion rates due to the increased rate of ionization of the metallic surface [34]. Furthermore, the presence of applied stresses can exacerbate the effect of the electric potential on the corrosion behavior of metallic materials [35]. In contrast, cathodic protection through applied potential can mitigate the corrosion rate of metallic materials [36].

Electrolyte concentration is another important potentiostatic parameter that can significantly affect the corrosion behavior of metallic materials. The concentration of electrolyte can influence the rate of ionization and diffusion of the metallic ions, which can affect the corrosion rate of metallic materials [36]. Higher electrolyte concentration can lead to more aggressive corrosion environments, whereas lower concentration can lead to a passivated or non-corrosive environment [37].

Overall, understanding the effects of potentiostatic parameters on corrosion is essential in developing corrosion prediction models and designing corrosion-resistant materials. As previously noted, this is not a trivial understanding, since many of the parameters that influence corrosion operate on probabilistic distributions and display nonlinear trends [13]. This project aims to capture these trends using the probabilistic modeling technique of PCA modeling, since this technique has shown to successfully model stochastic phenomena [30-32], including those in corrosion systems [15-16, 26-29].

CHAPTER 3

MATERIALS AND METHODS

This chapter of the thesis describes the experimental procedures and equipment utilized for studying the corrosion behavior of steel. This chapter provides a detailed overview of the experimental setup, including the sample preparation, corrosion testing, and data analysis methods. The materials used for sample preparation, as well as the properties and characteristics of the electrolyte solutions, are also presented. The PCA programming, correction, and validation methods are also provided. This chapter aims to provide a comprehensive description of the experimental techniques employed for the corrosion study and serves as a guide for researchers interested in similar studies.

3.1 Description of the Steel Specimens Used in the Study

For this study, the steel alloy used is AISI 1095 cold-rolled carbon steel. This specific alloy was selected for its combination of corrosion characteristics and mechanical properties. Though it has a higher carbon content than other steel alloys, it has been shown to have poor corrosion resistance [38, 39]. The goal of this study is to induce severe corrosion on the macroscopic scale in a short time period, so a poor corrosion resistance is preferrable. Considering mechanical properties, a material with a small plastic region on the stress-strain curve is desired. This is because the material will be subject to tensile testing later in model evaluation, and the results of the tensile test are most accurate when the material strains minimally before failing [40]. AISI 1095 is known to experience

brittle fracture due to its high carbon content, which increases its hardness and strength but also decreases its ductility and toughness [41].

Name	Plain Square	Circular Hole	Elliptical Hole	Dumbbell
Use	Parametric Study	Tensile Tests	Tensile Tests	Tensile Tests
Surface Area (in^2)	1.440	1.244	1.293	1.244
Total Edge Length (in.)	4.800	6.371	6.471	5.371
Image of Profile	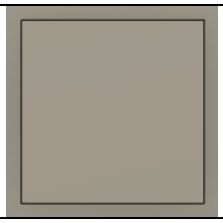	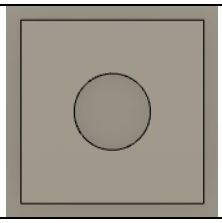	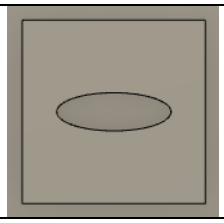	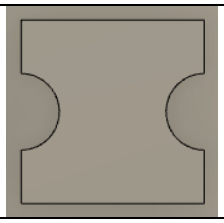

Table 1. Specimen designs used throughout the project.

The specimens are derived from a 0.050" thick stock sheet of AISI 1095 steel. Four different geometries are used in this project, defined by **Table 1**. The plain square geometry will be used in the parametric study, and the other three geometries will be used in the tensile tests. The tensile test geometries were chosen to induce stress concentrations, which are preferrable when tensile testing methods are involved [42]. All specimens are manufactured using the same method, which is CNC cutting on a ProtoMax OMAX abrasive water jet. The water jet uses high pressure water flow from a nozzle with a 0.046" diameter, 0.021" kerf width, and 0.039" head clearance. The cutting material used is an 80 media grit garnet abrasive. The specimen profiles were cut on the water jet, the pieces were separated by manually breaking them, and the edges were ground and polished. Although AISI 1095 is known to have a low machinability rating for carbon-containing steel [43], the specimens were produced quickly and with low variability due to the 0.050" sheet thickness and small amount of material removed.

3.2 Potentiostatic Corrosion Parameters Used in the Experiments

The controlled corrosion method used for this study is a three-electrode corrosion cell. The potentiostat used is a Gamry Instruments Interface 1010E, which has a wide range of testing availability, including electrochemical impedance spectroscopy (EIS). The method used for this study will be limited to potentiostatic experiments. The 1010E potentiostat has a maximum applied current of ±1 A, a maximum applied potential of ±12 V, and EIS range of 10 μHz - 2 MHz. Prior to any experimentation, the potentiostat is calibrated using a Gamry Instruments UDC4 (Universal Dummy Cell) and faraday cage according to a standard operating procedure in the Gamry Framework software.

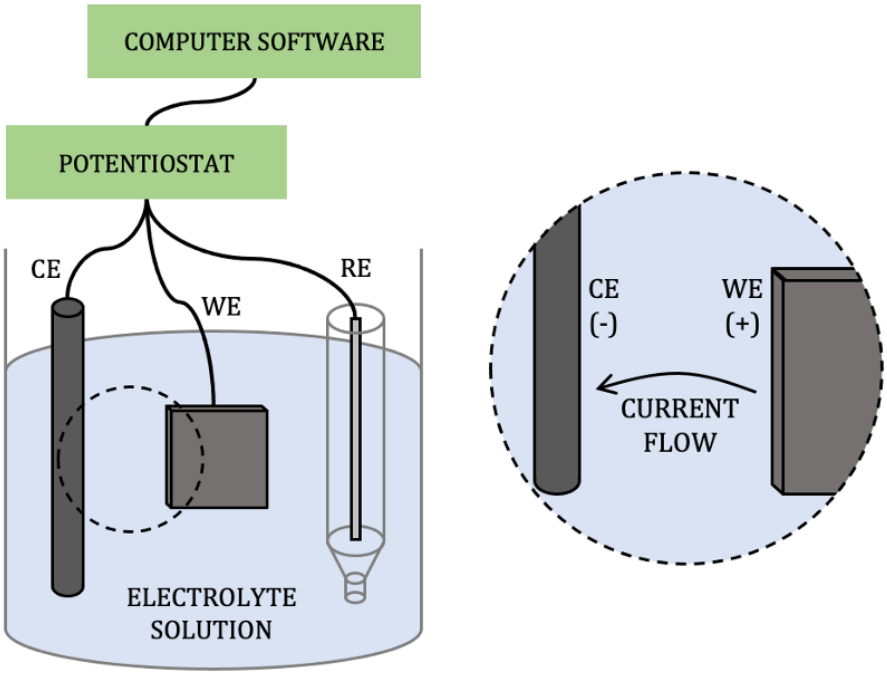

Figure 2. Three-electrode setup used in corrosion experiments.

The three-electrode corrosion cell consists of a working electrode (WE), counter electrode (CE), and reference electrode (RE). **Figure 2** pictures the complete three-electrode setup which is

used in all experiments. The WE is the electrode where the corrosion or electrochemical reaction of interest occurs [44, 45]. In this study, the WE is the AISI 1095 steel specimen. The WE is connected to the positive terminal of the potentiostat via six gold pogo pins in a metal ring, which evenly applies a current to the specimen. The CE is an electrode made of an inert material, which is graphite in this case, that does not participate in the reaction of interest. It is placed opposite the working electrode and connected to the negative terminal of the power supply or potentiostat. The CE provides a surface for the transfer of electrons to or from the electrolyte to balance the flow of current in the cell. The RE is an electrode with a known potential that serves as a reference for measuring the potential of the WE. It is made of a material with a stable and reproducible electrochemical potential, which is a silver-silver chloride electrode in this case.

The electrolyte solution used is saltwater, as it is the standard solution medium for numerous electrochemical corrosion studies [46]. The saltwater solution consists of lab-grade (99.9+% purity) sodium chloride and distilled, deionized water. The dissociated salt ions facilitate the exchange of electrons in the corrosion reaction [44], and aid in conducting the electric current flow simultaneously.

Element	C	Fe	Mn	P	S
Atomic Weight, W_i	12.011	55.845	54.938	30.974	32.065
Percent Composition, f_i	0.965	98.545	0.400	0.040	0.050
Most Stable Valence, n_i	4	3	2	2	3

Table 2. Alloy composition details for AISI 1095 steel.

The potentiostatic experiments are computer-controlled using a software provided by Gamry Instruments, called Gamry Framework. One important parameter required by the software is the equivalent weight of the WE material. The equivalent weight of the AISI 1095 is determined using the following equation, and the parameters listed in **Table 2.**

$$EW = \left(\sum_{i=1}^{n} \frac{n_i f_i}{W_i} \right)^{-1}$$

The parameters in **Table 2** are provided by the material supplier. For any percent compositions which were provided on a range, the mean value is used in the calculation. After setting up the software and preparing the corrosion cell, final parameters such as applied potential, solution concentration, and duration are defined by experiment matrices which are reflected in Appendix B. The equivalent weight is required to run any experiment, since it is used by the Gamry Framework software to calculate the amount of substance that is oxidized or reduced at the WE. By measuring the amount of charge passed during an electrochemical reaction and knowing the equivalent weight of the substance being oxidized or reduced, it is possible to calculate the number of moles of the substance involved in the reaction [44].

3.3 Overview of the MATLAB Programming

The PCA is developed in MATLAB, which is explained in-depth in the next chapter. This section will serve as an introduction to the modeling approach and will help set up the next section.

This modeling approach follows closely with some models for partial differential equations (PDEs). In computational engineering methods, it is often times preferrable to discretize PDEs and solve them numerically [47]. When a two-dimensional parabolic PDE is discretized, known functions govern the diffusion of one cell to its neighboring cells. These functions are often derived from statistical distributions, such as Maxwell-Boltzmann distributions used in chemical kinetics. Similarly, the governing rules in this PCA on probabilities and statistical distributions. The model simulates corrosion progression at the macroscale by defining a matrix of cells that represent the material surface. With every iteration, each cell is assigned a set of probabilities for corrosion propagation. The probabilities are based on environmental conditions such as temperature,

humidity, and exposure to corrosive agents, as well as material properties such as composition, microstructure, and defects. The progression of corrosion is determined by iteratively applying the probabilities to each cell and its neighboring cells. PCA models are based on a statistical approach that considers the inherent variability processes [48], such as corrosion propagation in this case. The probabilities used in the model can be calibrated using experimental data, which is discussed in the next section.

For this study, a parameter is defined which encapsulates these statistical distributions and describes the rate of corrosion of the specimens. This parameter is referred to as the corrosion propagation constant, denoted by *P*, and is directly related to the rate at which corrosion propagates across the surface of the specimen. The inputs to the MATLAB model include a value for *P*, duration, and an image of the initial surface. The duration is used to determine the number of iterations performed in the model, and the initial surface image is used as a boundary condition. The outputs include mass loss (as a percentage), maximum pitting depth, and a heatmap of the predicted final surface. Analysis of the outputs for different values of *P* is the method for calibrating the model.

3.4 Parametric Study Used for Model Correction

A parametric study is performed to characterize a relationship between the corrosion propagation constant, *P*, and physical parameters which are known to affect the rate of corrosion. In potentiostatic cases, these parameters may include temperature, electric potential, electrolyte concentration, electrolyte pH, and elemental composition of the WE [44, 45]. This study focuses on electric potential and electrolyte concentration. A higher applied potential may lead to an increased corrosion rate, while a lower applied potential may reduce the rate of corrosion [49]. Electrolyte concentration can also affect the rate of corrosion as it can affect the availability of reactants and the

transport of ions to the electrode surface. Studies have shown that increasing the concentration of the electrolyte can lead to an increase in the corrosion rate, while decreasing the concentration can decrease the rate of corrosion [50]. It is important to study the effect of these parameters to understand the mechanism of corrosion and to develop effective strategies to model it.

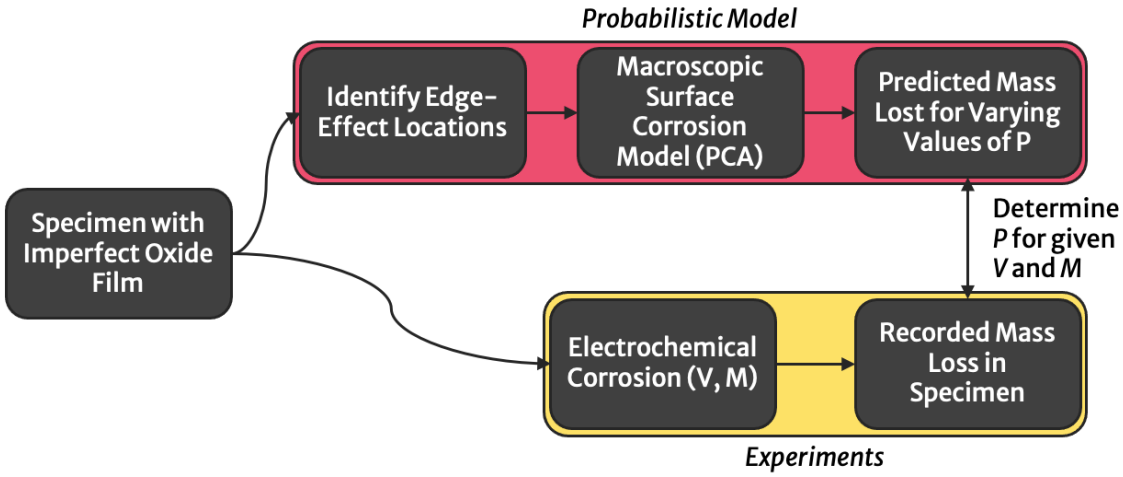

Figure 3. Scheme for parametric study.

Two sets of experiments are performed, each isolating one of the independent variables of interest. The parameters of these experiments, and their results, can be found in Appendix B. For each experiment, the percentage of mass lost is recorded for the given electric potential and solution concentration. The PCA is iteratively executed for different values of *P* until a similar percent mass loss is predicted. The relative error for the correlating mass loss is 5%. Since the model is probabilistic, there are some inherent variations to the predicted mass loss. This variation in output values is found to be 1-3% under the input parameters used in this project. However, in all calculations involving the PCA, the results of ten simulations are averaged and used. **Figure 3** is a flow diagram which describes this scheme.

After all the experimental data is collected, multiple nonlinear regression is performed based on trends displayed in each of the studies. Once a relationship is developed between the corrosion propagation rate and the parameters of applied potential and solution concentration, the MATLAB model inputs may be changed for future use.

3.5 Tensile Testing Methods Used for Model Evaluation

Tensile tests are used in part to evaluate the accuracy of the PCA model. Corroded specimens will be subject to the tensile tests and the results will be compared to simulated results based on the output from the PCA. This section outlines the details of the tensile testing methods.

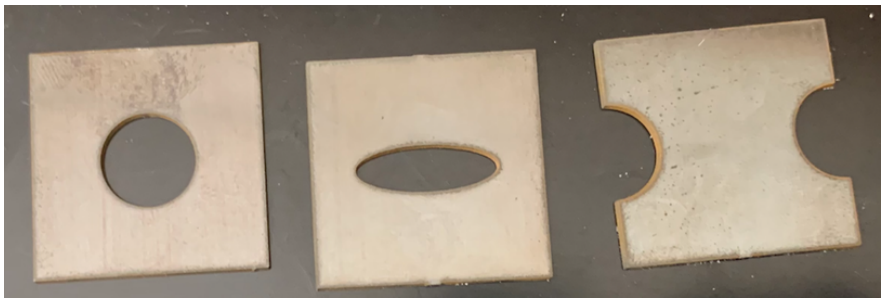

Figure 4. Image of specimens used in tensile tests.

Tensile tests are performed on an MTS Landmark Servohydraulic Test System with the stress concentration specimens shown in **Figure 4**. The test specimens are secured by two hydraulic wedges that use a clamping pressure of 1000 psi. Each wedge grip clamps a 0.2" section of the test specimen, which provides sufficient space between the clamps and the stress concentration geometry. Once the specimen is clamped in place, a strain may be applied by the machine. The strain rate used in this study is 0.25 mm per second, or 0.0098" per second. This tensile testing procedure adheres to the methods in ASTM A370 save the geometry specifications.

For each of the three specimen geometries, tensile tests are performed for a set of corroded specimens and a set of control specimens that are not subject to potentiostatic corrosion. The

specimens that are corroded are subject to the same potentiostatic conditions (described in §3.2) used on those in the parametric study. For all corroded tensile specimens, the potentiostatic parameters are set to a duration of 3.00 hours, an applied potential of 1.00 volts, and an electrolyte concentration of 3.00 mol/L. This selection falls within the bounds parametric study and yields a significant amount of material loss.

3.6 FEA Methods Used for Model Evaluation

FEA is performed to simulate the tensile tests described in the last section, using specimen models derived from the output of the PCA model. The results of the FEA simulations are compared to the tensile test results to evaluate the accuracy of the PCA model. This section outlines the details of the FEA method and parameters.

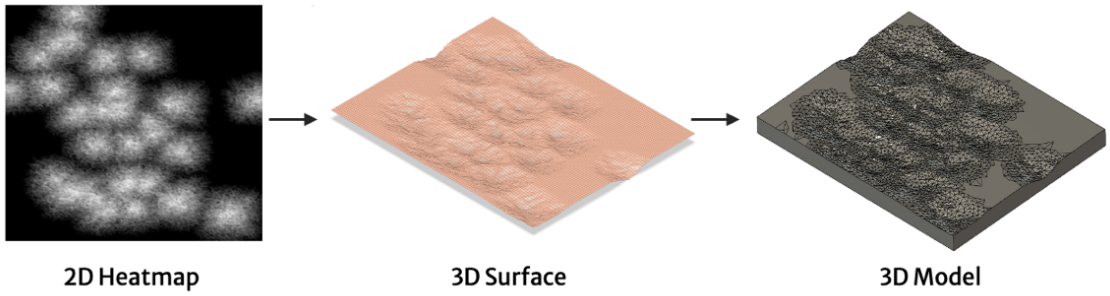

Figure 5. Method for corroded model derivation.

FEA is performed using the Static Structural system model in Ansys Workbench 2023 R1. Control geometries (circular hole, elliptical hole, and dumbbell) are used, as well as their simulated corroded counterparts, which are derived from the PCA model. The PCA model exports a 2D heatmap of the corrosion intensity, which may be converted to a 3D surface. This 3D surface is manually converted to a 3D model, and the full process is depicted in **Figure 5**. Meshes for the models are generated in Ansys under the same parameters, and the details are included in Appendix

E. Mesh defeaturing is disabled and the smoothing parameter is set to the lowest setting to preserve the corrosion topology. A convergence study is performed for each simulation to confirm that the mesh density sufficiently converges on a solution. It is evident that the simulated corrosion from the PCA is carried over into the Ansys models, since the element counts in the corroded model meshes is significantly higher than the element counts in the control model meshes.

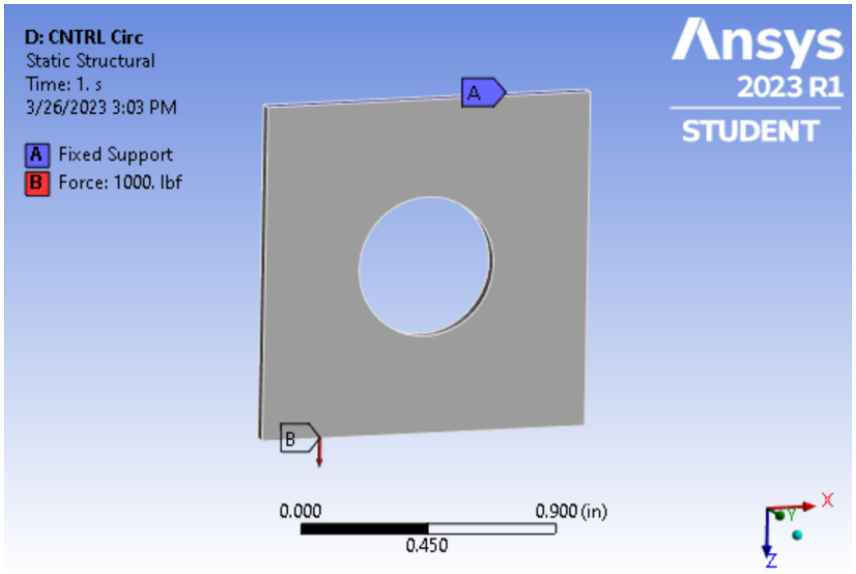

Figure 6. Loading scheme for simulated tension tests.

In the Static Structural model, one end of the specimen is fixed, and the opposite end is loaded under a constant force of 1000 lbf. This loading scheme is depicted in **Figure 6**. These boundary conditions approximate the same physics from the tensile tests described in §3.5.

	Metric Units	SI Units
Density	7.85 g/cm^3	0.284 lbm/in^3
Young's Modulus	200,000 MPa	29,000 ksi
Poisson's Ratio	0.3	0.3
Bulk Modulus	167,000 MPa	24200 ksi
Shear Modulus	76,900 MPa	11200 ksi
Tensile Yield Strength	517 MPa	75.0 ksi
Tensile Ultimate Strength	685 MPa	99.4 ksi

Table 3. Material properties for AISI 1095 steel used in FEA.

The parameters in **Table 3** are provided by the material supplier. For any properties which were provided on a range, the mean value is used in the simulations. Failure analysis using Explicit Dynamics system is not available under the Ansys student license, so conclusions are drawn from static analysis results out of necessity. The standard Ansys Mechanical APDL solver is used to solve the Static Structural system in each case. The output results, which are listed in Appendix E, include the stress intensity, equivalent stress, and directional deformation of the model. Any trends in these results will be compared to trends observed in the tensile tests.

CHAPTER 4

PROBABILISTIC CELLULAR AUTOMATA DEVELOPMENT

In this chapter, the approach to developing the PCA will be described. Each section will discuss key aspects of the model. Firstly, it is important to outline the assumptions made by the model. The assumptions serve to simplify the model and specify all of the mechanics that are involved. Any assumptions that are unclear will be explained further in the following sections. The PCA model assumptions include:

i. Surface is perfectly planar.
ii. Surface is not subject to any stresses.
iii. Microscopic corrosion phenomena (~1nm) are negligible.
iv. All electrochemical parameters are constant and time-invariant.
v. Oxide film layer perfectly protects underlying bulk metal from corrosion.
vi. Corrosion of specimen is limited to only the normal anodic surface of the WE.
vii. Corroded material initially propagates from seed points.
viii. All corrosion seed points are known.
ix. Seed points are located along all edges of the material.
x. Corroded material fully dissolves in solution and disappears from the surface model.
xi. Spreading of corroded material is dependent on status of neighbors.
xii. Penetration of corroded material is dependent on status of neighbors.

xiii. Both spreading and penetration of corroded material are dependent on a probabilistic distribution which is a function of electrochemical parameters.

4.1 Modeling Overview

The primary model inputs are a user-defined value for the corrosion propagation constant (*P*), a value for the total time spent in the corrosion cell, and an image of the initial surface. The user-defined value for *P* is initially chosen iteratively based on model outputs but is eventually given based on the parametric study with known values for electric potential and solution concentration. This is described further in §4.3. The value for time is used to determine the number of iterations for which the model is run; in this model, one minute in the corrosion chamber equates to one iteration.

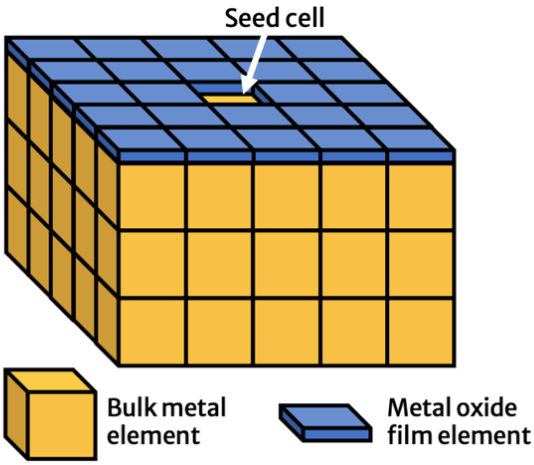

Figure 7. Simplified discrete surface model.

The first step is to discretize the initial surface into 0.1 mm by 0.1 mm square cells. This is done by compressing the initial surface image to a state where each pixel measures 0.1 mm across and converting this compressed image into a matrix. Some of these cells will serve as "seed" cells, or those from which corrosion will initially propagate from. The corrosion initiation sites, or seed cells,

are based on the edge effect. The edge effect is a phenomenon observed in corrosion studies where corrosion is more severe in edges of the material [51-54]. This is commonly because subtractive manufacturing processes (i.e., cutting) destroy the metal oxide film and expose a significant amount of the bulk metal. A simplified model is shown in **Figure 7**, which indicates that seed cells come from breaches in the metal oxide film. In the PCA, seed cell locations are characterized as the edges of the metal specimen, which are identified through image processing operations.

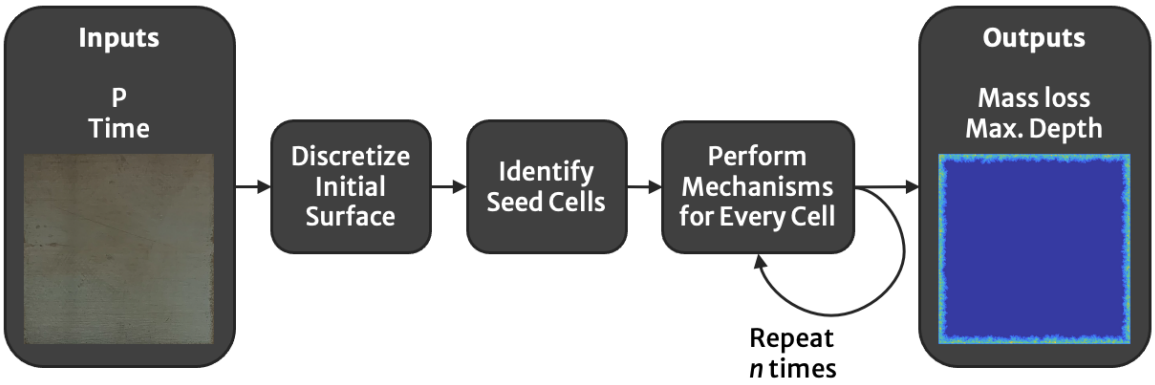

Figure 8. Programming overview for PCA.

Once the seed cell locations are known, the surface matrix will undergo changes based on rulesets that are applied locally. The rulesets describe the propagation of corrosion, which consists of both spreading (across the surface) and penetration (into surface). These rulesets will be described in §4.2. The ruleset will be applied to every cell in the surface for the specified number of iterations.

The model outputs include: the percent mass loss, the maximum depth, and a plot of the final surface. In the model, it is assumed that when material is corroded, it disappears from the metal surface. This assumption makes the calculations for the percent mass loss and maximum depths trivial calculations.

4.2 Explanation of the Rules Used in the Model

One of the most critical aspects of any cellular automata model is the implementation of a neighborhood. In CA modeling, a neighborhood refers to the adjacent cells that surround a given cell in a lattice or grid. The neighborhood defines which cells are considered in the local interactions of the CA model. The size and shape of the neighborhood can vary depending on the specific CA model being used and the nature of the system being modeled. Some common neighborhood models are shown in **Figure 9**. The selection of a neighborhood is an important aspect of CA modeling, as it affects the behavior and properties of the system being modeled [55, 56]. The PCA used in this project uses a Moore neighborhood, since all cells should consider interactions with all adjacent neighbors. Furthermore, the Moore neighborhood is simpler to program compared to other neighborhood models.

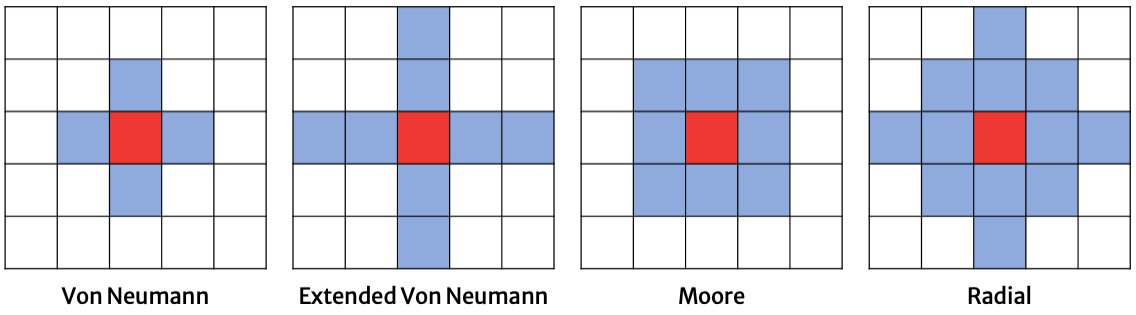

Figure 9. Various neighborhoods traditionally used in CA models.

The metal surface is assumed to be planar and is modeled by a "2.5D" second-order tensor. Each cell inherently contains locational data by its position in the matrix. The value that each cell holds contains information on its state of corrosion. These states may be either corroded or not corroded. If the state is corroded, the cell will carry information on how severe the corrosion is, which is related to the depth at that location. If the state is not corroded, the cell will not have a

direct effect on its neighbors. **Figure 10** depicts the neighborhood model which is used, and it outlines the numeric values which are assigned to the cells that indicate these states.

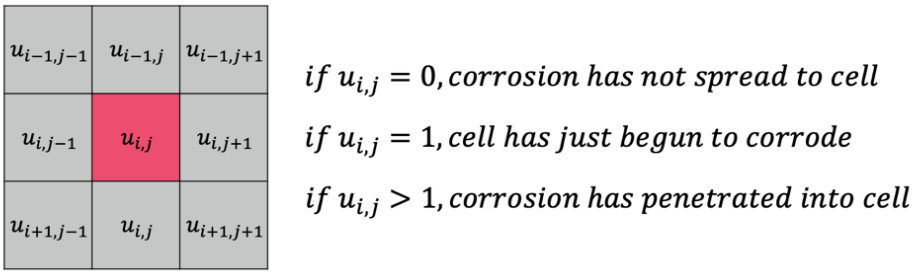

Figure 10. Corrosion status values used in PCA.

Figure 11 depicts a cross-section of the surface model (from **Figure 7**) with an arbitrary assignment of values to some cells. This is meant to provide clarity on the link between **Figure 10** and **Figure 7**. Any cells assigned with a value of zero indicate that corrosion has not spread to that cell, and any assigned with a positive integer value can be directly linked to the amount of material missing from that location using the model resolution.

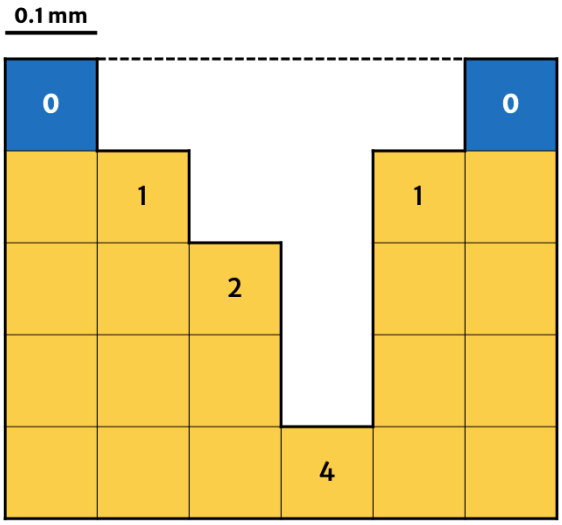

Figure 11. Cross-section of an arbitrary iteration of the surface model.

In this model, both the spread of corrosion (transition from 0 to 1 in a cell) and the penetration of corrosion (increase in value above 1 in a cell) are equally dictated by the status of their neighbors and are additionally dictated by a probability statement. In other words, all corrosion propagation is determined locally (assumptions x and xi). This indicates that both spreading and penetration are equally likely to occur. The probability statement dependence (assumption xii) is how the model becomes probabilistic, and it is why a value for the corrosion propagation constant, *P*, is required. The probability defined by *P* is applied as an additional logic statement to every interaction between adjacent cells.

4.3 Description of the Multiple Nonlinear Regression Used for Model Correction

Experimental data is used to describe the relationship between *P* and the electrochemical parameters V and *M*. To accomplish this, the PCA is repeatedly executed using interpolating values of *P* until a similar percent mass loss is predicted. The relative error for the correlating mass loss between the PCA and the electrochemical experiments is 5%. Since the model is probabilistic, there are variations to the predicted mass loss which are determined to be 1-3%. To account for this, the model is executed ten times under a value of *P*, and the average of the predicted mass loss is used.

The predicted mass loss from the PCA output is used in comparison to experimental results to determine a corresponding value for *P* under the V and *M* from the given experiment. Appendix B outlines the data that is collected in this manner. §5.1 and Appendix C contain the results of the multiple nonlinear regression using this experimental data.

CHAPTER 5

RESULTS

This chapter presents the results from both the parametric study and the mechanical evaluation. The parametric study involves the results of the electrochemical experiments and PCA model outputs, and the mechanical evaluation involves the results of the tensile tests and FEA results.

5.1 Summary of the PCA Model and its Predictions

Based on the results of the parametric study, it is determined that *P* has a cubic polynomial relationship with *V*, and an exponential relationship with *M*. These trends are shown in **Figure 12** and **Figure 13**, respectively. One discovery was that the PCA model automatically captured the scaling effect of time in extended simulations. This is evident by similar values of *P* in experiments with identical electrochemical parameters but different durations.

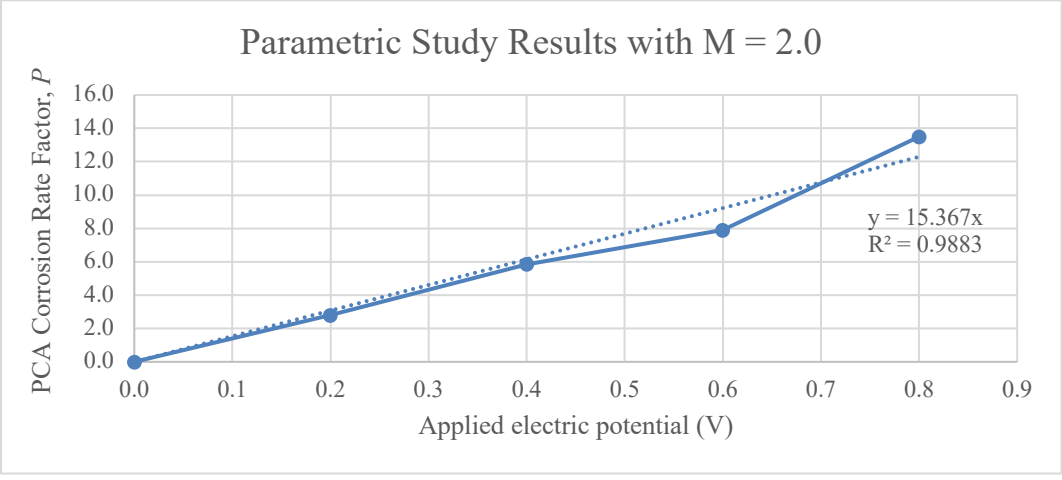

Figure 12. Parametric study results with constant concentration.

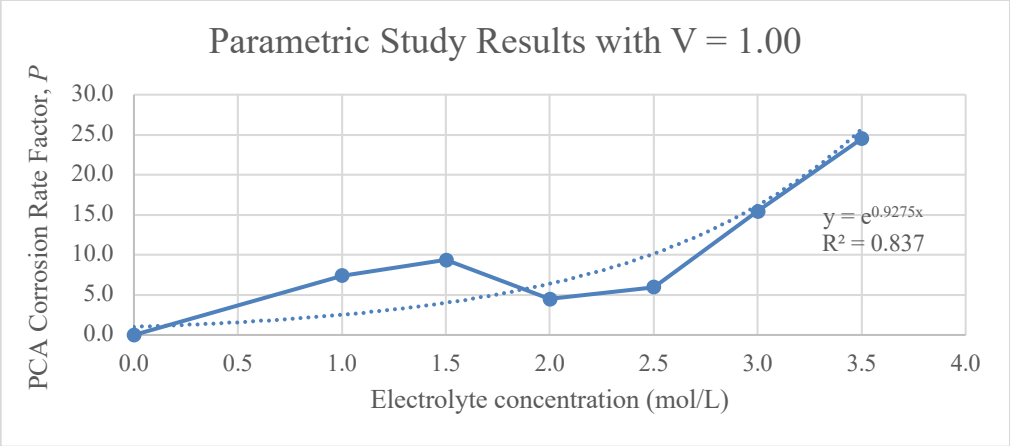

Figure 13. Parametric study results with constant voltage.

Considering the trends shown in the parametric study, a mathematical model for *P* is created, and a multiple nonlinear regression is performed using the experimental data (entries 1-18 in Appendix B). The multiple nonlinear regression is executed for many different models, and these results are presented in **Table 4**. The root mean square error (RMSE) is also provided alongside each model to indicate its accuracy relative to the other models. Many different combinations and permutations were considered for this study. Some equations were generated using combinations of others which had relatively low values for RMSE.

Model Equation	RMSE	A	B	C	D	E	F
$P = \frac{Ae^{BM} + C}{V + D} + Ve^{EM} + F$	3.395	-0.5665	-142.19	-0.1127	-0.8171	0.8761	2.3212
$P = Ve^{AM} + B$	3.546	0.8682	2.4952	-	-	-	-
$P = AVe^{BM} + C$	3.738	1.0512	0.8542	2.4217	-	-	-
$P = Ae^{BM} + CV + D$	3.960	0.7247	0.9524	5.7884	-2.5420	-	-
$P = (Ae^{BM} + C)(V + D)$	3.961	0.5170	0.9524	2.3158	0.4017	-	-
$P = \frac{Ae^{BM}}{V + C}$	4.440	43291	0.8711	38897	-	-	-
$P = \frac{Ae^{BM} + C}{V + D}$	4.514	2690.3	1.4894	92216	23700	-	-

Table 4. Multiple nonlinear regression results of different model equations.

From these models, the result with the lowest RMSE is selected to calibrate the PCA. The details for this regression result are found in Appendix C, and the resulting equation is plotted in **Figure 14**. This mathematical model may be integrated into the PCA model in place of the input parameter *P*. In other words, the PCA will require applied voltage (*V*) and electrolyte concentration (*M*) as user inputs instead of *P*. This removes the need to iteratively run the PCA for different values of *P* to obtain anticipated results.

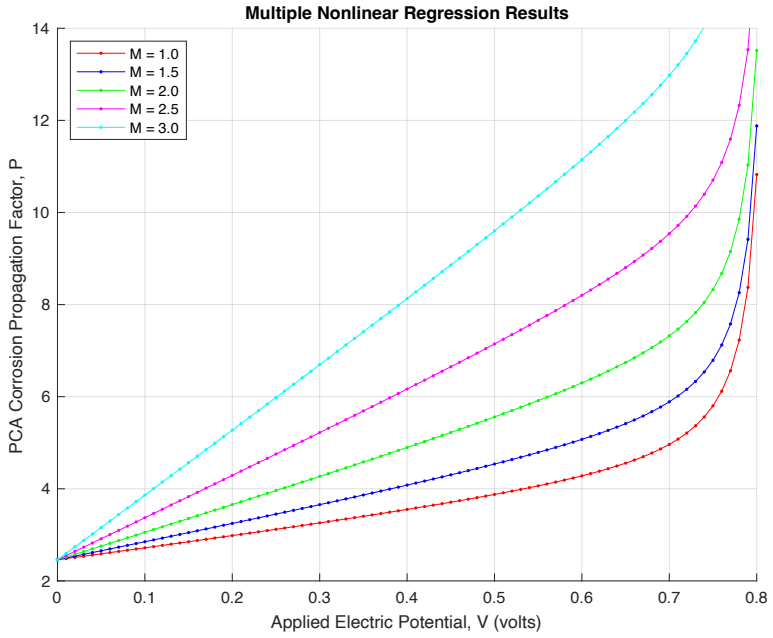

Figure 14. Multiple nonlinear regression results.

Additional experiments (entries 19-21 in Appendix B) are performed to evaluate the accuracy of this mathematical model.

5.2 Summary of the Experimental and FEA Results

The tensile tests were performed on specimens which were subject to potentiostatic corrosion, and specimens which were not. The results were averaged for the corroded and non-corroded results, for the three different geometries.

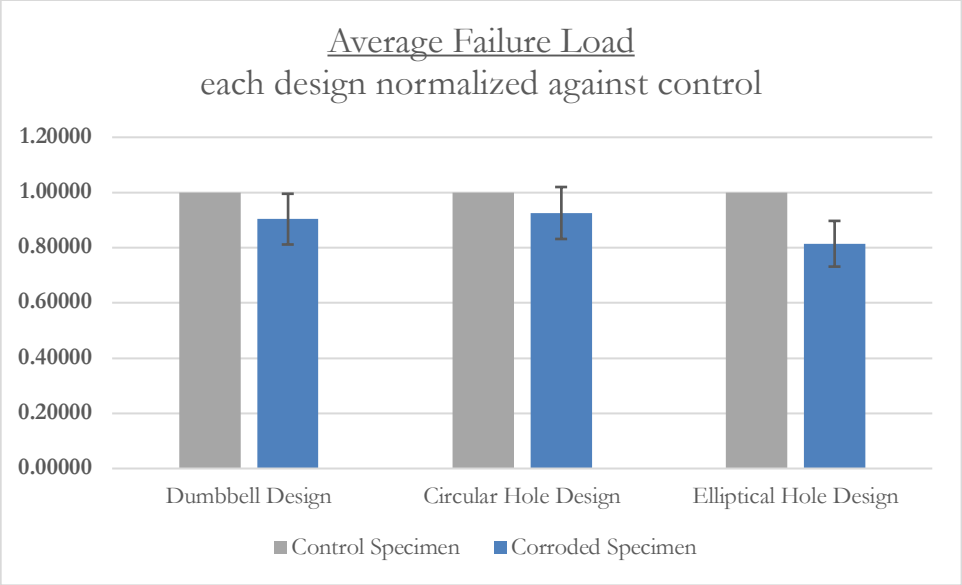

Figure 15. Average failure load from tensile tests.

As expected, the average failure load decreases in all specimen designs when corroded. **Figure 15** shows that when normalized, it is shown that the elliptical hole design specimen is the most affected by the corrosion in terms of tensile failure load change.

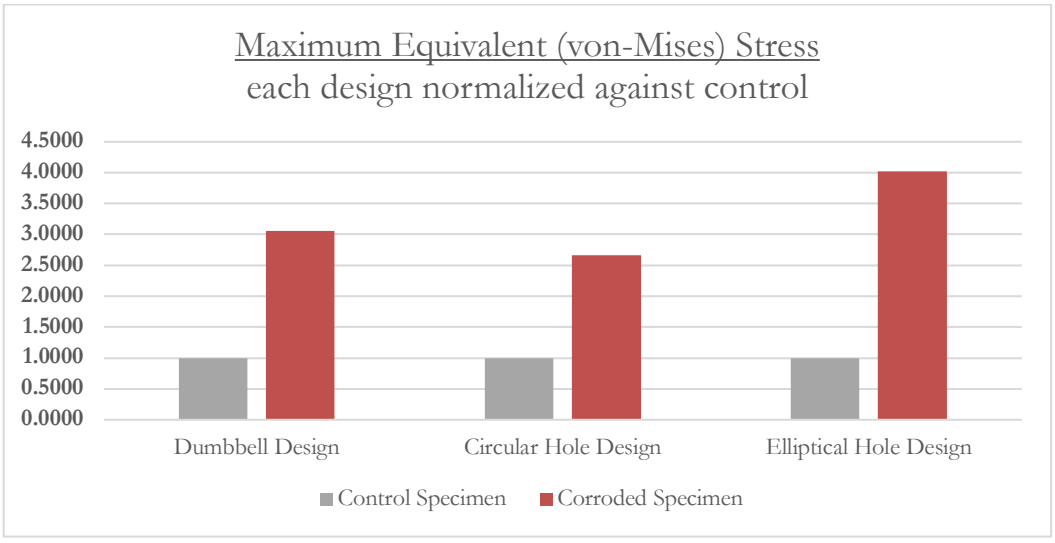

Figure 16. Maximum equivalent stress from FEA.

As expected, the simulated corrosion from the PCA significantly increases the maximum equivalent stress in each case under identical loading. This is expected, as the corroded material is known to introduce stress concentrations [57-59]. **Figure 16** plots the normalized results and shows that the elliptical hole design is the most sensitive to the corrosion process in terms of maximum equivalent stress increase.

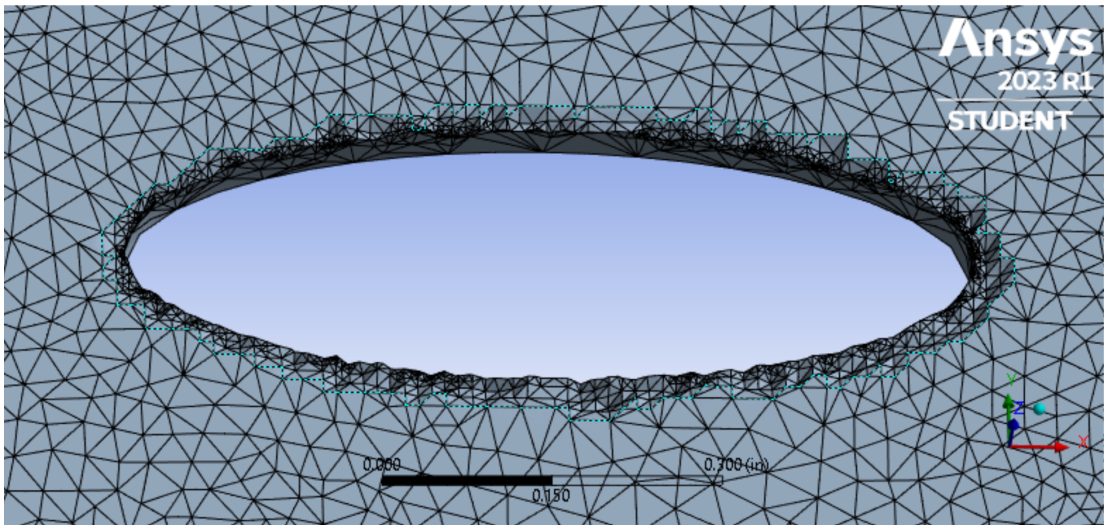

Figure 17. Mesh showing the simulated corroded material at the edges of a specimen.

The simulated corrosion introduces sharp changes in material topography, which can be seen in the mesh shown in **Figure 17**. All corroded meshes derived from the PCA contain a substantially large number of elements compared to their control counterparts, which is indicative of the erratic topography which was induced at the edges of the specimens.

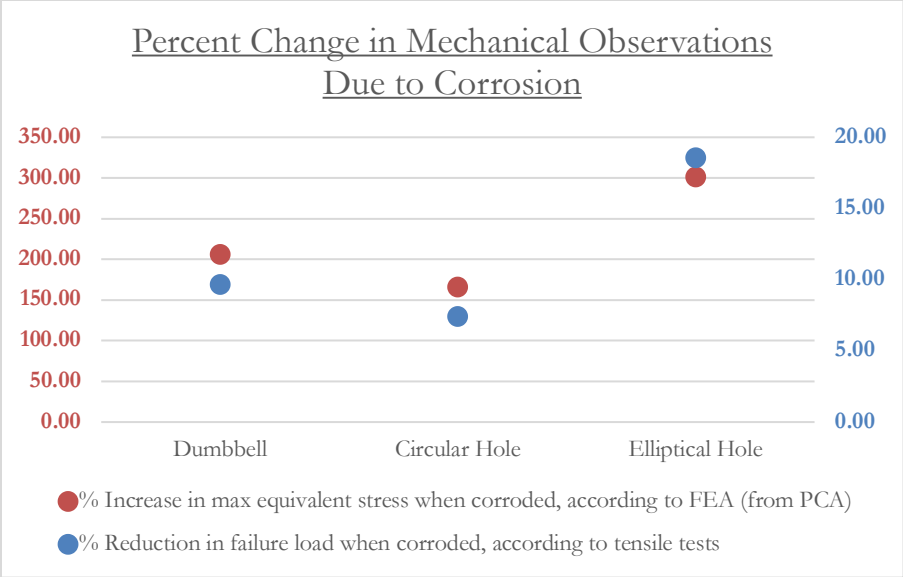

Figure 18. Percent change in mechanical observations.

Figure 18 compares the similar trends which are shown in the tensile tests and FEA. Maximum stress and failure load are expected to have an opposing relationship, so simply the percent changes are compared. Considering the data from the tensile tests (colored blue), it is observed that the elliptical hole design is most susceptible to changes caused by corrosion, followed by the dumbbell design and finally the circular hole design. Similarly, considering the data from the FEA results (colored red), we see the same trend; the elliptical hole design is most sensitive to changes induced by the corrosion process, followed by the dumbbell and circular hole designs.

It was originally theorized that the elliptical hole design was most sensitive to the corrosion because this design had the longest total edge length (found in **Table 1**) of the three designs. In theory, this should mean that there are the most seed cells per specimen which might induce the most corrosion under the edge effect assumption. However, there is no geometric correlation regarding area or perimeter with the results shown in **Figure 18**.

These mechanical observations, maximum equivalent stress and failure load, show similar trends across varying specimen geometries even though each set of trends come from entirely unrelated sets of data. From this, it is concluded that the macroscopic corrosion model was successful in predicting the complex trends associated with corrosion-induced reduction in strength.

CHAPTER 6

CONCLUSIONS

The PCA shows great promise in simulating macroscopic corrosion, especially in terms of material loss and mechanical characteristics. The nonlinear model does well in determining the rate of corrosion based on the potentiostatic parameters of applied voltage and solution concentration, as the model is compared to results which were not used in its development. These results compare closely to the model prediction, except for the data point at a solution concentration of 4.00 M. This may be in part due to the probabilistic nature of the PCA, but is more likely because the regression was performed using data for solution concentration from 0.00 M to 3.00 M.

The results from the mechanical evaluation are especially promising because trends align between the FEA results, where the models are derived from the PCA, and the tensile tests. Not only did the trends in relative change in mechanical properties due to corrosion align, but they did so across very different specimen geometries. That is, the trends were captured even amidst the varying specimen designs and inherent unpredictability associated with corrosion.

6.1 Limitations and Future Directions for Research

Many limitations for the PCA come from the modeling assumptions, such as the likelihood for penetration or spreading of corroded material. Currently, both are equally likely, but this may not always be accurate. Under certain conditions, extreme pitting is likely to occur, which would make penetration the more likely mechanism. A solution to this could be using a more accurate input for

the initial surface to the PCA. A 3D scanning or photogrammetry method could be used to provide more accurate initial topography at a higher resolution than a digital image.

Another limitation of the model is to predict the effects of corrosion when there are seed cells that are not positioned on a geometric edge. A solution to this could be to artificially superimpose seed cells onto the initial surface of the metal. This may be done thoughtfully or by means of a random distribution. **Figure 19** shows the results of artificial insertion of seed cells into a square specimen. The artificially inserted seed cells contribute to the corrosion of the specimen and display interactions with the edge effect seed cells. The seed cell insertion schema is as follows:

a) No artificially inserted seed cells.

b) Evenly spaced grid of 100 artificially inserted seed cells.

c) Random distribution of 100 artificially inserted seed cells.

d) Random distribution of 1000 artificially inserted seed cells.

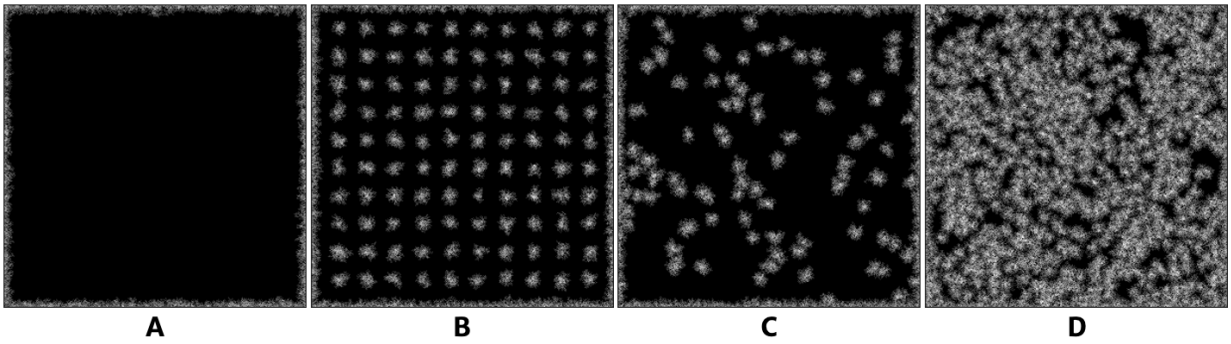

Figure 19. Results of PCA with artificially inserted seed cells.

Randomly inserted cells can mimic physical anomalies which would otherwise initiate corrosion propagation, such as an impurity in the alloy or a microscopic crack. If the frequency of these anomalies is approximately known, randomly inserting them in this manner may yield more

accurate results, especially in macroscopic terms like overall mass loss and reduction in mechanical strength.

Another limitation of the PCA is the ability to predict topologies where the entire surface cannot be seen from the direction of the planar surface normal. In other words, the PCA cannot model overhanging features. This type of topology is commonly seen in pitting corrosion models. These topologies are characterized by a film perforation which opens up underneath the surface to a void, where the void has a larger projected area than the perforation. For this PCA, it is assumed that the impact of these overhanging features are negligible, considering the macroscopic model scale.

Some future considerations could include extra data collection for the parametric study. Another future consideration could be to investigate other factors which were not considered. In the parametric study, only applied potential and solution concentration are considered. However, it may be desired to study the effects of temperature, different metals, or different solutions.

Another future consideration could be to investigate the effect of alternate manufacturing methods on the spread of corrosion across the surface. Rather than cutting specimens from stock material, it would be insightful to see whether changing this would have a significant effect. For example, in additive manufacturing, there will not be edges exposed in the same way, and the modeling approach may break down. Extra manufacturing factors to consider in this case include printing scheme and heat treatment.

6.2 Implications for Mechanical Engineering and Materials Science

The PCA modeling approach shows great promise in engineering for its ability to describe complex and stochastic phenomena such as corrosion propagation.

In general, the development of a reliable probabilistic macroscopic corrosion model has significant implications for the field of mechanical engineering and materials science. With such a model, engineers and scientists can more accurately predict the behavior of corroding metals in various environments and conditions, leading to improved design and maintenance strategies for steel structures. This information is crucial in the design of corrosion-resistant materials and structures, which can lead to substantial economic savings by reducing maintenance and repair costs [60]. Additionally, the ability to predict corrosion rates and behavior can improve the safety of structures, as corrosion-related failures can be catastrophic. The use of probabilistic models can provide a more comprehensive understanding of the variability and uncertainty inherent in corrosion behavior, allowing for more accurate risk assessments and structural design [61]. Overall, the development of a reliable probabilistic macroscopic corrosion model has the potential to greatly benefit the fields of mechanical engineering and materials science by improving the design, maintenance, and safety of steel structures.

REFERENCES

[1] Koch, G., Varney, J., Thompson, N., Moghissi, O., Gould, M., & Payer, J. (2016). International measures of prevention, application, and economics of corrosion technologies study. *NACE international*, *216*, 2-3.

[2] National Transportation Safety Board, & United States. National Transportation Safety Board. (2008). *Collapse of I-35W Highway Bridge, Minneapolis, Minnesota, August 1, 2007*. Createspace Independent Pub.

[3] Díez-Pérez, I., Sanz, F., & Gorostiza, P. (2006). In situ studies of metal passive films. *Current Opinion in Solid State and Materials Science*, *10*(3-4), 144-152.

[4] Strehblow, H. H. (2002). Mechanisms of pitting corrosion. *CORROSION TECHNOLOGY-NEW YORK AND BASEL-*, *17*, 243-286.

[5] Revie, R. W., & Uhlig, H. H. (2008). Corrosion and corrosion control. A John Wiley & Sons. *Hoboken, New Jersey*, *399*.

[6] Makhlouf, A. S. H., & Aliofkhazraei, M. (Eds.). (2015). *Handbook of materials failure analysis with case studies from the chemicals, concrete and power industries*. Butterworth-Heinemann.

[7] Roberge, P. R. (2008). *Corrosion engineering*. McGraw-Hill Education.

[8] Liu, M. (2021). Effect of uniform corrosion on mechanical behavior of E690 high-strength steel lattice corrugated panel in marine environment: A finite element analysis. *Materials Research Express*, *8*(6), 066510.

[9] Chen, H., Zhang, J., Yang, J., & Ye, F. (2018). Experimental investigation into corrosion effect on mechanical properties of high strength steel bars under dynamic loadings. *International Journal of Corrosion*, *2018*.

[10] Guo, X. Y., Kang, J. F., Zhu, J. S., & Duan, M. H. (2019). Corrosion behavior and mechanical property degradation of weathering steel in marine atmosphere. *Journal of Materials in Civil Engineering*, *31*(9), 04019181.

[11] Pidaparti, R. M., & Rao, A. S. (2008). Analysis of pits induced stresses due to metal corrosion. *Corrosion Science*, *50*(7), 1932-1938.

[12] Svintradze, D. V., & Pidaparti, R. M. (2010). A theoretical model for metal corrosion degradation. *International Journal of Corrosion*, *2010*, 1-7.

[13] Codaro, E. N., Nakazato, R. Z., Horovistiz, A. L., Ribeiro, L. M. F., Ribeiro, R. B., & Hein, L. D. O. (2002). An image processing method for morphology characterization and pitting corrosion evaluation. *Materials Science and Engineering: A*, *334*(1-2), 298-306.

[14] Lishchuk, S. V., Akid, R., Worden, K., & Michalski, J. (2011). A cellular automaton model for predicting intergranular corrosion. *Corrosion Science*, *53*(8), 2518-2526.

[15] Pérez-Brokate, C. F., Di Caprio, D., Féron, D., de Lamare, J., & Chaussé, A. (2017). Probabilistic cellular automata model of generalised corrosion, transition to localised corrosion. *Corrosion Engineering, Science and Technology*, *52*(sup1), 186-193.

[16] Cui, C., Ma, R., Chen, A., Pan, Z., & Tian, H. (2019). Experimental study and 3D cellular automata simulation of corrosion pits on Q345 steel surface under salt-spray environment. *Corrosion Science*, *154*, 80-89.

[17] Eddy, N. O., Momoh-Yahaya, H., & Oguzie, E. E. (2015). Theoretical and experimental studies on the corrosion inhibition potentials of some purines for aluminum in 0.1 M HCl. *Journal of Advanced Research*, *6*(2), 203-217.

[18] Stipaničev, M., Turcu, F., Esnault, L., Schweitzer, E. W., Kilian, R., & Basseguy, R. (2013). Corrosion behavior of carbon steel in presence of sulfate-reducing bacteria in seawater environment. *Electrochimica Acta*, *113*, 390-406.

[19] Chen, M. C., Wen, Q. Q., Zhu, Q., Huang, H., & Xie, L. (2017). Simulation of corrosion process for concrete filled steel tubular columns with the cellular automata method. *Engineering Failure Analysis*, *82*, 298-307.

[20] Caleyo, F., Velázquez, J. C., Valor, A., & Hallen, J. M. (2009). Probability distribution of pitting corrosion depth and rate in underground pipelines: A Monte Carlo study. *Corrosion Science*, *51*(9), 1925-1934.

[21] Rocabruno-Valdés, C. I., González-Rodriguez, J. G., Díaz-Blanco, Y., Juantorena, A. U., Muñoz-Ledo, J. A., El-Hamzaoui, Y., & Hernández, J. A. (2019). Corrosion rate prediction for metals in biodiesel using artificial neural networks. *Renewable Energy*, *140*, 592-601.

[22] Biezma, M. V., Agudo, D., & Barron, G. (2018). A Fuzzy Logic method: Predicting pipeline external corrosion rate. *International Journal of Pressure Vessels and Piping*, *163*, 55-62.

[23] Wen, Y. F., Cai, C. Z., Liu, X. H., Pei, J. F., Zhu, X. J., & Xiao, T. T. (2009). Corrosion rate prediction of 3C steel under different seawater environment by using support vector regression. *Corrosion Science*, *51*(2), 349-355.

[24] Mairesse, J., & Marcovici, I. (2014). Around probabilistic cellular automata. *Theoretical Computer Science*, *559*, 42-72.

[25] Grinstein, G., Jayaprakash, C., & He, Y. (1985). Statistical mechanics of probabilistic cellular automata. *Physical review letters*, *55*(23), 2527.

[26] Pérez-Brokate, C. F., Di Caprio, D., Féron, D., De Lamare, J., & Chaussé, A. (2014). Overview of cellular automaton models for corrosion. In *Cellular Automata: 11th International Conference on Cellular Automata for Research and Industry, ACRI 2014, Krakow, Poland, September 22-25, 2014. Proceedings 11* (pp. 187-196). Springer International Publishing.

[27] Urda, D., Luque, R. M., Jiménez, M. J., Turias, I., Franco, L., & Jerez, J. M. (2013). A constructive neural network to predict pitting corrosion status of stainless steel. In *Advances in Computational Intelligence: 12th International Work-Conference on Artificial Neural Networks, IWANN 2013, Puerto de la Cruz, Tenerife, Spain, June 12-14, 2013, Proceedings, Part I 12* (pp. 88-95). Springer Berlin Heidelberg.

[28] Fatoba, O. O., Leiva-Garcia, R., Lishchuk, S. V., Larrosa, N. O., & Akid, R. (2018). Simulation of stress-assisted localised corrosion using a cellular automaton finite element approach. *Corrosion Science*, *137*, 83-97.

[29] Lishchuk, S. V., Akid, R., Worden, K., & Michalski, J. (2011). A cellular automaton model for predicting intergranular corrosion. *Corrosion Science*, *53*(8), 2518-2526.

[30] Marco, D. E., Páez, S. A., & Cannas, S. A. (2002). Species invasiveness in biological invasions: a modelling approach. *Biological Invasions*, *4*, 193-205.

[31] Zamith, M., Leal-Toledo, R. C. P., Clua, E., Toledo, E. M., & de Magalhães, G. V. (2015). A new stochastic cellular automata model for traffic flow simulation with drivers' behavior prediction. *Journal of computational science*, *9*, 51-56.

[32] Li, X., & Yeh, A. G. O. (2001). Calibration of cellular automata by using neural networks for the simulation of complex urban systems. *Environment and Planning A*, *33*(8), 1445-1462.

[33] Pérez-Brokate, C. F., Di Caprio, D., Féron, D., De Lamare, J., & Chaussé, A. (2017). Pitting corrosion modelling by means of a stochastic cellular automata-based model. *Corrosion Engineering, Science and Technology*, *52*(8), 605-610.

[34] Paul, S. C., Babafemi, A. J., Conradie, K., & van Zijl, G. P. (2017). Applied voltage on corrosion mass loss and cracking behavior of steel-reinforced SHCC and mortar specimens. *Journal of Materials in Civil Engineering*, *29*(5), 04016272.

[35] Zhu, L. Y., Cui, Z. Y., Cui, H. Z., Wang, X., & Li, Y. Z. (2022). The effect of applied stress on the crevice corrosion of 304 stainless steel in 3.5 wt% NaCl solution. *Corrosion Science*, *196*, 110039.

[36] Li, D. G., Wang, J. D., Chen, D. R., & Liang, P. (2014). Influences of pH value, temperature, chloride ions and sulfide ions on the corrosion behaviors of 316L stainless steel in the simulated cathodic environment of proton exchange membrane fuel cell. *Journal of Power Sources*, *272*, 448-456.

[37] Wang, Y., Jiang, S. L., Zheng, Y. G., Ke, W., Sun, W. H., & Wang, J. Q. (2012). Electrochemical behaviour of Fe-based metallic glasses in acidic and neutral solutions. *Corrosion science*, *63*, 159-173.

[38] McGuire, Michael F. *Stainless steels for design engineers*. ASM International, 2008.

[39] Dwivedi, D., Lepková, K., & Becker, T. (2017). Carbon steel corrosion: a review of key surface properties and characterization methods. *RSC advances*, *7*(8), 4580-4610.

[40] Paul, S. K., Sivaprasad, S., Dhar, S., & Tarafder, S. (2011). Key issues in cyclic plastic deformation: experimentation. *Mechanics of materials*, *43*(11), 705-720.

[41] Lemaitre, J. (Ed.). (2001). *Handbook of materials behavior models, three-volume set: nonlinear models and properties*. Elsevier.

[42] Pilkey, W. D., Pilkey, D. F., & Bi, Z. (2020). *Peterson's stress concentration factors*. John Wiley & Sons.

[43] Davim, J. P. (Ed.). (2011). *Machining of hard materials*. Springer Science & Business Media.

[44] Zoski, C. G. (Ed.). (2006). *Handbook of electrochemistry*. Elsevier.

[45] Mansfeld, F. (2003). Electrochemical methods of corrosion testing. *ASM handbook*, *13*, 446-462.

[46] Melchers, R. E. (2003). Effect on marine immersion corrosion of carbon content of low alloy steels. *Corrosion Science*, *45*(11), 2609-2625.

[47] Chopard, B., Dupuis, A., Masselot, A., & Luthi, P. (2002). Cellular automata and lattice Boltzmann techniques: An approach to model and simulate complex systems. *Advances in complex systems*, *5*(02n03), 103-246.

[48] Valor, A., Caleyo, F., Rivas, D., & Hallen, J. M. (2010). Stochastic approach to pitting-corrosion-extreme modelling in low-carbon steel. *Corrosion Science*, *52*(3), 910-915.

[49] Frankel, G. S. (2016). Fundamentals of corrosion kinetics. *Active protective coatings: new-generation coatings for metals*, 17-32.

[50] Wang, S., Gu, Y., Geng, Y., Liang, J., Zhao, J., & Kang, J. (2020). Investigating local corrosion behavior and mechanism of MAO coated 7075 aluminum alloy. *Journal of Alloys and Compounds*, *826*, 153976.

[51] Ogle, K., Baudu, V., Garrigues, L., & Philippe, X. (2000). Localized electrochemical methods applied to cut edge corrosion. *Journal of the Electrochemical Society*, *147*(10), 3654.

[52] Simillion, H., Van den Steen, N., Terryn, H., & Deconinck, J. (2016). Geometry influence on corrosion in dynamic thin film electrolytes. *Electrochimica Acta*, *209*, 149-158.

[53] Trinh, D., Dauphin Ducharme, P., Mengesha Tefashe, U., Kish, J. R., & Mauzeroll, J. (2012). Influence of edge effects on local corrosion rate of magnesium alloy/mild steel galvanic couple. *Analytical chemistry*, *84*(22), 9899-9906.

[54] Wang, D. D., Liu, X. T., Su, Y., Wu, Y. K., Yang, Z., Han, H. P., ... & Shen, D. J. (2020). Influences of edge effect on microstructure and corrosion behaviour of PEO coating. *Surface Engineering*, *36*(2), 184-191.

[55] Berto, F., & Tagliabue, J. (2012). Cellular automata.

[56] Preston Jr, K., & Duff, M. J. (2013). *Modern cellular automata: theory and applications*. Springer Science & Business Media.

[57] Jia, C., Shao, Y., Guo, L., & Huang, H. (2021). Surface topography and stress concentration analysis for corroded high strength steel plate. *Journal of Constructional Steel Research*, *187*, 106952.

[58] Kantzos, C., Lao, J., & Rollett, A. (2019). Design of an interpretable Convolutional Neural Network for stress concentration prediction in rough surfaces. *Materials Characterization*, *158*, 109961.

[59] Li, A., Wang, H., Li, H., Kong, D., & Xu, S. (2022). Stress Concentration Analysis of the Corroded Steel Plate Strengthened with Carbon Fiber Reinforced Polymer (CFRP) Plates. *Polymers*, *14*(18), 3845.

[60] Taylor, C. D., Lu, P., Saal, J., Frankel, G. S., & Scully, J. R. (2018). Integrated computational materials engineering of corrosion resistant alloys. *npj Materials Degradation*, *2*(1), 6.

[61] Contreras, G., Goidanich, S., Maggi, S., Piccardi, C., Vittoria Diamanti, M., Pedeferri, M. P., & Lazzari, L. (2011). Representing localized corrosion processes through cellular automata.

APPENDICES

MATLAB Code

```
function [d_max,A_ratio,pm_loss] = CorrosionPCA_Hampson(img_fn,output_fn,mstart,width,ratio,iter,P)
% Daniel Hampson, 2023
% Probabilistic Cellular Automata model for corrosion propagation,
% initiated by the edge effect.
%   Takes an image of a steel specimen and applies it to a PCA. An initial
%   imperfection surface is generated and serves as the first boundary
%   condition.
%   Input:  image file name, ex. img_fn = 'test piece.png'
%           output filename, ex. output_fn = 'results.png'
%           width of specimen, in millimeters
%           ratio for image processing contrast, closer to 1 means more sensitive
%           iteration number, which is time elapsed. Note 1 iter = 1 min.
%           P, corrosion propagation constant
%   Output: maximum depth in surface, predicted
%           ratio of final corrosion area to initial imperfection area
%           mass lost, predicted loss in specimen mass
%           final surface contours as grayscale PNG, saved to output_fn
%% Prepare image
I0 = imread(img_fn);
pixels = ceil(width*10); %sets each pixel to be 0.1mm in width
I0 = imresize(I0, [pixels pixels]);
I2 = histeq(I0);
I3 = rgb2gray(I2);
Max = nanmax(I3,[],'all');
Min = nanmin(I3,[],'all');
[i,j] = size(I3);
% Identify edges using contrasting background
for a = 1:i
    for b = 1:j
        if I3(a,b) <= (Max/ratio)
            I3(a,b) = 255;
        else
            I3(a,b) = 0;
        end
    end
end
I3(1:i,1) = 255; I3(1:i,j) = 255; I3(1,1:j) = 255; I3(i,1:j) = 255;
%Note: Defect present = 1, no surface defects = 0
s0 = rot90(I3')/255;
figure(4)
pcolor(s0)
shading('interp')
title('Initial Surface')
colorbar('Ticks',[0,1],'TickLabels',{'No Defect','Defect Present'})
c = 0; %counter
disp(' --> image processing complete')
%% Cellular Automata
s1 = im2double(s0);
[i,j] = size(s1);
for a = 1:i
    for b = 1:j
        if s1(a,b) > 0
            s1(a,b) = 1;
        elseif s1(a,b) <= 0
            s1(a,b) = 0;
        end
    end
end
s0 = s1;
disp(' --> conversion to matrix complete')
%Trim to square matrix (back-up)
```

```
while ~(i==j)
    if i > j
        s1(1,:) = [];
    elseif j > i
        s1(:,1) = [];
    end
    [i,j] = size(s1);
end
cell_width_mm = width/i; %mm
cell_width_nm = cell_width_mm*10^6; %nm
disp(' --> beginning CA')
while c < iter
    s2 = s1;
    for a = 2:i-1
        for b = 2:i-1
        nh = [s1(a-1,b-1) s1(a-1,b) s1(a-1,b+1);... %neigborhood
              s1(a,b-1)   s1(a,b)   s1(a,b+1);...
              s1(a+1,b-1) s1(a+1,b) s1(a+1,b+1)];
        Logic1 = nh > nh(2,2);
        Logic2 = nh == nh(2,2);
        if sum(sum(nh)) > 1
            if (Logic1(1,1) || Logic2(1,1)) && (rand<=P)
                s2(a,b) = s1(a,b) + 1;
            elseif (Logic1(1,2) || Logic2(1,2)) && (rand<=P)
                s2(a,b) = s1(a,b) + 1;
            elseif (Logic1(1,3) || Logic2(1,3)) && (rand<=P)
                s2(a,b) = s1(a,b) + 1;
            elseif (Logic1(2,1) || Logic2(2,1)) && (rand<=P)
                s2(a,b) = s1(a,b) + 1;
            elseif (Logic1(2,3) || Logic2(2,3)) && (rand<=P)
                s2(a,b) = s1(a,b) + 1;
            elseif (Logic1(3,1) || Logic2(3,1)) && (rand<=P)
                s2(a,b) = s1(a,b) + 1;
            elseif (Logic1(3,2) || Logic2(3,2)) && (rand<=P)
                s2(a,b) = s1(a,b) + 1;
            elseif (Logic1(3,3) || Logic2(3,3)) && (rand<=P)
                s2(a,b) = s1(a,b) + 1;
            end
        end
        end
    end
    c = c + 1;
    s1 = s2;
end
final_result = s2*cell_width_mm;
disp(' --> CA complete')
%% Plot the Heatmap for comparison
figure(5)
pcolor(final_result)
shading('interp')
title('Final Surface')
c = colorbar;
c.Label.String = 'Depth (mm)';
xlabel('Pixel X-Location')
ylabel('Pixel Y-Location')
%% Plot Mesh of Surface
X = 1:i;
Z = -1*double(final_result);
figure(6)
mesh(X,X,Z)
daspect([1 1 1])
%% Calculate maximum depth
d_max = max(max(final_result)) %mm
%% Calculate initial and final affected area
s3 = zeros(i);
for a = 1:i
    for b = 1:i
        if s2(a,b) > 0
            s3(a,b) = 1;
        end
    end
end
Area_i = sum(sum(s0))*cell_width_mm^2;
AiFrac = Area_i/(cell_width_mm*i)^2;
Area_f = sum(sum(s3))*cell_width_mm^2;
AfFrac = Area_f/(cell_width_mm*i)^2;
A_ratio = Area_f/Area_i
%% Calculate predicted mass lost
```

```
V_loss = (sum(sum(s2))-sum(sum(s0)))*cell_width_mm^3;
rho = .00785; % g/mm^3, density of steel
mloss = V_loss*rho; %g
pm_loss = 100*mloss/mstart % predicted %mass lost for parametric study
%% Write Result Image to File
% imwrite(final_result,output_fn,'PNG')
%% End PCA
disp(' --> finished')
end
```

Potentiostatic Experimental Data

Exp #	Time (hrs)	V (volts)	M (mol/L)	Initial Mass (g)	Final Mass (g)	Mass Lost (g)	Mass Lost (%)	Corresponding value of *P* (*10^-4)
1	1.50	0.200	2.00	9.380	9.374	0.006	0.064	3.2
2	3.00	0.200	2.00	9.380	9.369	0.011	0.117	2.4
3	1.50	0.400	2.00	9.261	9.240	0.021	0.227	5.1
4	3.00	0.400	2.00	9.261	9.230	0.031	0.335	6.6
5	1.50	0.600	2.00	9.377	9.360	0.017	0.181	8.3
6	3.00	0.600	2.00	9.377	9.340	0.037	0.395	7.5
7	1.50	0.800	2.00	9.337	9.309	0.028	0.300	12.5
8	3.00	0.800	2.00	9.337	9.239	0.098	1.050	14.5
9	1.50	1.000	1.00	9.343	9.330	0.013	0.139	6.2
10	3.00	1.000	1.00	9.343	9.300	0.043	0.460	8.6
11	1.50	1.000	1.50	9.389	9.365	0.024	0.256	10.9
12	3.00	1.000	1.50	9.389	9.350	0.039	0.415	7.8
13	1.50	1.000	2.50	9.343	9.330	0.013	0.139	6.8
14	3.00	1.000	2.50	9.343	9.322	0.021	0.225	5.1
15	1.50	1.000	3.00	9.310	9.265	0.045	0.483	17.4
16	3.00	1.000	3.00	9.310	9.224	0.086	0.924	13.5
17	1.50	1.000	3.50	9.343	9.250	0.093	0.995	28.2
18	3.00	1.000	3.50	9.343	9.180	0.163	1.745	20.8
19	0.50	0.500	4.00	9.326	9.325	0.001	0.011	29.5
20	0.50	0.200	3.00	9.347	9.276	0.071	0.760	10.9
21	0.50	0.800	2.00	9.331	9.254	0.077	0.825	13.0

Multiple Nonlinear Regression Parameters and Results

Summary Statistics

Variable	Observations	Minimum	Maximum	Mean	Std. deviation
P	12	0.000	24.500	8.100	6.982
V	12	0.000	1.000	0.750	0.363
M	12	0.000	3.500	1.958	0.891

Correlation Matrix

Variable	V	M	P
V	**1.000**	-0.035	0.455
M	-0.035	**1.000**	0.689
P	0.455	0.689	**1.000**

Goodness of Fit Statistics

Statistic	Full
Observations	12.000
DF	6.000
SSE	69.149
MSE	11.525
RMSE	3.395
AIC	35.016
AICC	63.016
Iterations	38.000

Model Equation

$$P = \frac{Ae^{BM} + C}{V + D} + Ve^{EM} + F$$

Model Parameters

Parameter	Value	Standard error	Lower bound (95%)	Upper bound (95%)
A	-0.5665	0.786	-2.489	1.356
B	-142.1942	0.000	-142.194	-142.194
C	-0.1127	0.295	-0.835	0.609
D	-0.8171	0.047	-0.932	-0.702
E	0.8761	0.054	0.744	1.008
F	2.3212	1.396	-1.094	5.736

Predictions and Residuals

Observation	V	M	P	Pred(P)	Residuals
Obs1	0.00	2.0	0.001	2.465	-2.464
Obs2	0.20	2.0	2.800	3.657	-0.857
Obs3	0.40	2.0	5.850	4.898	0.952
Obs4	0.60	2.0	7.900	6.300	1.600
Obs5	0.80	2.0	13.500	13.516	-0.016
Obs6	1.00	0.0	0.001	0.019	-0.018
Obs7	1.00	1.0	7.400	4.106	3.294
Obs8	1.00	1.5	9.350	5.426	3.924
Obs9	1.00	2.0	4.500	7.472	-2.972
Obs10	1.00	2.5	5.950	10.641	-4.691
Obs11	1.00	3.0	15.450	15.553	-0.103
Obs12	1.00	3.5	24.500	23.165	1.335

Tensile Testing Data

Tensile Test #	Specimen Design	Corrosion Experiment #	Peak Load (lbf.)	Ultimate Strain (in.)
1	Dumbbell	N/A (Control)	9504.739	0.046
2	Dumbbell	N/A (Control)	11579.788	0.043
3	Dumbbell	N/A (Control)	12899.881	0.058
4	Circular Hole	N/A (Control)	10760.011	0.055
5	Circular Hole	N/A (Control)	11082.471	0.043
6	Circular Hole	N/A (Control)	10616.861	0.047
7	Elliptical Hole	N/A (Control)	8025.399	0.034
8	Elliptical Hole	N/A (Control)	6870.989	0.033
9	Elliptical Hole	N/A (Control)	7660.676	0.033
10	Elliptical Hole	22	5233.406	0.031
11	Elliptical Hole	23	6909.257	0.033
12	Elliptical Hole	24	6226.122	0.032
13	Circular Hole	25	10579.295	0.048
14	Circular Hole	26	9063.630	0.047
15	Circular Hole	27	10406.549	0.048
16	Dumbbell	28	9219.493	0.050
17	Dumbbell	29	11106.979	0.065
18	Dumbbell	30	10379.356	0.051

FEA Model Parameters and Results

Important Meshing Parameters

Physics Preference	Mechanical
Resolution	2
Mesh Defeaturing	No
Smoothing	Low
Inflation Option	Smooth Transition
Transition Ratio	0.272
Maximum Layers	5
Growth Rate	1.2

Results from Simulations with Control Models

		Circular Hole	Elliptical Hole	Dumbbell
Mesh Statistics	Nodes	1474	1614	899
	Elements	182	202	108
Element Quality Statistics	Min	0.64238	0.29145	0.50178
	Max	0.89910	0.90062	0.78492
	Average	0.83009	0.84409	0.68475
Aspect Ratio Statistics	Min	1.5561	1.4722	2.0000
	Max	2.8605	4.2257	3.4918
	Average	1.8619	1.7614	2.5127
Solution Results	Max Equivalent Stress (psi)	69202	1.55E+05	5.40E+04
	Max Directional Deformation (in.)	0.0012947	0.0017566	0.0012486

Results from Simulations with PCA-Derived Models

		Circular Hole	Elliptical Hole	Dumbbell
Mesh Statistics	Nodes	29438	31016	28523
	Elements	15575	16347	15085
Element Quality Statistics	Min	0.04068	0.04065	0.03045
	Max	0.98867	0.98499	0.99207
	Average	0.51830	0.50672	0.51913
Aspect Ratio Statistics	Min	1.2211	1.2562	1.2159
	Max	80.5570	72.7870	81.1640
	Average	3.8314	4.0249	3.8010
Solution Results	Max Equivalent Stress (psi)	1.84E+05	6.21E+05	1.65E+05
	Max Directional Deformation (in.)	0.0013456	0.0018391	0.0013645